NANO LETTERS

LETTER

pubs.acs.org/NanoLett

A Scheme for Detecting Every Single Target Molecule with Surface-Enhanced Raman Spectroscopy

Eric C. Le Ru,*[,†] Johan Grand,*[,‡] Idrissa Sow,[‡] Walter R. C. Somerville,[†] Pablo G. Etchegoin,[†] Mona Treguer-Delapierre,[¶] Gaëlle Charron,[‡] Nordin Félidj,[‡] Georges Lévi,[‡] and Jean Aubard[‡]

[†]The MacDiarmid Institute for Advanced Materials and Nanotechnology, School of Chemical and Physical Sciences, Victoria University of Wellington, P.O. Box 600, Wellington 6140, New Zealand

[‡]Université Paris Diderot, Sorbonne Paris Cité, ITODYS, UMR CNRS 7086, 15 rue J-A de Baïf, 75205 Paris Cedex 13, France

[¶]CNRS, Université de Bordeaux, ICMCB, 87 av. du Dr. A. Schweitzer, 33608 Pessac Cedex, France

Supporting Information

ABSTRACT: Surface-enhanced Raman spectroscopy (SERS) is now a well-established technique for the detection, under appropriate conditions, of single molecules (SM) adsorbed on metallic nanostructures. However, because of the large variations of the SERS enhancement factor on the surface, only molecules located at the positions of highest enhancement, so-called hot-spots, can be detected at the single-molecule level. As a result, in all SM-SERS studies so far only a small fraction, typically less than 1%, of molecules are actually observed. This complicates the analysis of such experiments and means that trace detection via SERS can in principle still be vastly improved. Here we propose a simple scheme, based on selective adsorption of the target analyte at the SERS hot-spots only, that allows in principle detection of *every* single target molecule in solution. We moreover provide a general experimental methodology, based on the comparison between average and maximum (single molecule) SERS enhancement factors, to verify the efficiency of our approach. The concepts and tools introduced in this work can readily be applied to other SERS systems aiming for detection of every single target molecule.

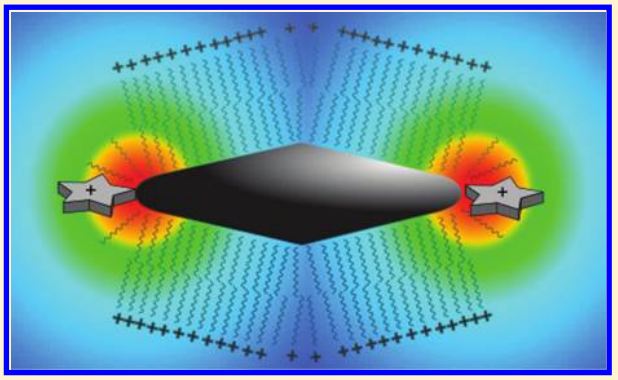

KEYWORDS: Surface-enhanced Raman spectroscopy, single molecule detection, plasmonics, site-selective adsorption, CTAB bilayer, bianalyte SERS

Two independent reports[1,2] in 1997 on the observation of single molecule (SM) detection using surface-enhanced Raman spectroscopy (SERS)[3,4] triggered a renewed interest in this technique.[5−11] It meant that SERS enhancement factors (EFs) were in principle sufficiently large to promote Raman spectroscopy to the coveted club of "single-molecule optical detection techniques", as fluorescence had done many years earlier.[12−14] Although these initial reports claimed SERS EFs as large as 10^{14}, it was later realized[15,16] that SERS EFs in the range $10^{8}-10^{10}$ were more typical of SM-SERS. Such values are much more in agreement with electromagnetic calculations of the SERS EFs.[17,18] They also led to the realization that SM-SERS detection was possible even for nonresonant molecules[19,20] and for resonant molecules with SERS EFs as low as $10^{5}-10^{6}$.[21]

Early studies[1,2,15] used ultralow concentration of analytes as a proof for SM-SERS detection and relied on the random adsorption of these molecules at the site of highest SERS EF on the substrate (so-called hot-spots). These hot-spots (HSs) however represent a very small proportion of the total surface area for adsorption, typically less than 1%[22−24] and the use of ultralow concentration results in an extremely poor statistics of SM-SERS events. The bianalyte SERS method,[22] which uses a mixture of two preferably chemically similar but Raman-distinguishable analytes, was developed to remedy this problem and has been further perfected with the use of isotopologues as bianalyte SERS partners.[25,26] The technique permits the use of higher concentrations (and therefore provides a much larger number of SM-SERS events), while preserving the ability to ensure, at least statistically, the SM nature of the events. This has allowed a more systematic study of the phenomenology of SM-SERS[27,28] and SM-SERS is now used as a tool to study the properties of single molecules in various contexts, for example their electrochemistry,[29] resonant Raman spectra,[30] conduction[31] and heating properties,[32] or homogeneous Raman broadening.[33]

The SM-SERS problematic as it stands is schematically summarized in Figure 1, where the three steps (by increasing difficulty) are presented: (I) Demonstration of SM-SERS capabilities using ultralow analyte concentration, as in the early studies. (II) Routine detection of many SM-SERS events for further studies, as allowed for example by the bianalyte SERS method. Yet, this

Received: August 31, 2011
Revised: October 4, 2011
Published: October 10, 2011

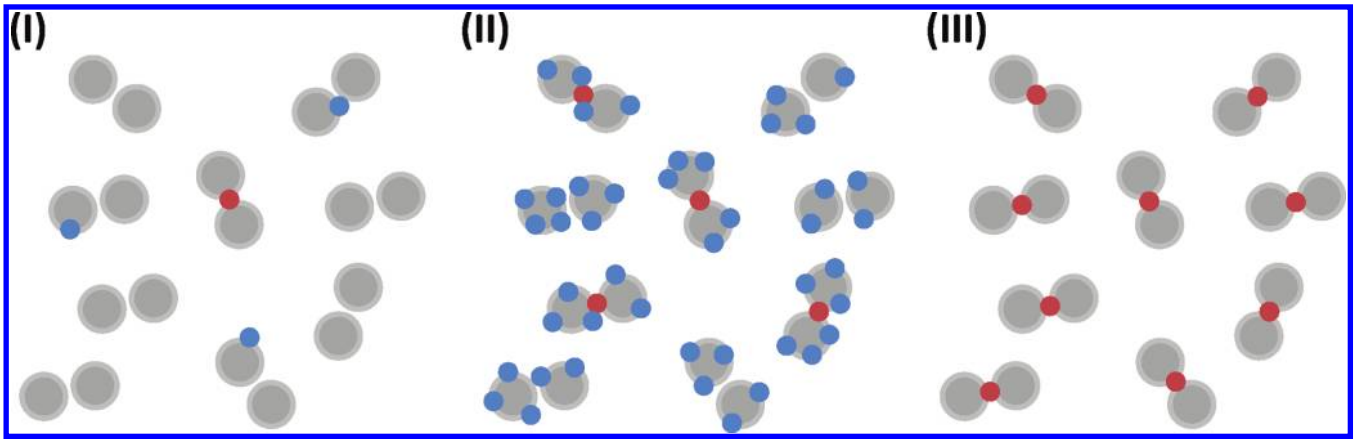

Figure 1. Progression of the SM-SERS problematic. The dimer conveniently represents a typical SERS substrate with a hot-spot in the gap, but a similar schematics could be drawn for single elongated nanoparticles with hot-spots at their tips (as studied here). Dots represent molecules, either SERS-active (red) when adsorbed at hot-spots, or SERS-inactive (blue) elsewhere. The first challenge for SM-SERS was the demonstration of SM-detection capabilities, using ultralow concentrations (I). Next, the study of the SM-SERS phenomenology (II) requires a larger statistics of SM-SERS events, which can be achieved using larger concentrations in a method such as bianalyte SERS. The ultimate goal is the observation of every single molecule with SERS (III) and this is the subject of this work.

still relies on random adsorption of some molecules at hot-spots, while the majority adsorbs elsewhere and does not contribute to the SERS signals. The next logical step forward is therefore (III) routine detection of every single molecule, which requires to devise a scheme where every molecule (in a solution for example) would adsorb at a hot-spot (see Figure 1III), where it can in principle be detected via SERS. Tip-enhanced Raman spectroscopy (TERS)[34−36] arguably represents the earliest attempt to achieve this, albeit with obvious sampling difficulties. Recent efforts have focused on methods to improve the monodispersity of hot-spots in solution, by fabricating nanoparticle (NP) aggregates with well-defined geometries[37−39] and with an accurate control of the gap dimensions.[40−45] Attempts to "build the SERS hot-spot around the target molecule", an approach akin to TERS, have also been recently reported.[39,45,46] The possibility of site-selective adsorption of the target analyte at the hot-spot for SERS (an arguably more practical approach), has also been very recently demonstrated by Chen et al. using gold nanorods.[47,48] Although these studies focused only on ensemble SERS measurements, that is, many-molecules and many-aggregates, they provide a glimpse of the possibilities that site-selective adsorption of the target analyte at the hot-spot may offer. In fact, such an approach provides a promising pathway to achieving the situation represented in Figure 1III and this is precisely what our work aims to demonstrate. In this report, we therefore provide an example of such a general methodology to implement III, based on the principle of chemically blocking access of the analyte to the surface, except at the hot-spots. We explicitly demonstrate its efficacy by comparing average and maximum (single molecule) SERS EFs, which incidentally provides a simple and experimentally accessible figure of merit against which future schemes could be tested. The scheme is shown to be ultimately capable of detecting via SERS every molecule of the target analyte present in the solution at the single molecule level. This study moreover provides an experimental confirmation of the possibility of detecting SM-SERS signals with SERS EFs as low as 10^6, and as a corollary, that SM-SERS detection is possible on single metallic NPs (as opposed to gap-containing structures).

Sample Characterization. As a model example of implementation of this scheme, we have used solutions of colloidal gold bipyramids (BiP) capped with a bilayer of cethyltrimethylamonium bromide (CTAB). The gold BiPs in solution are synthesized using a seed-mediated route in the presence of CTAB surfactants.[49] After synthesis the gold BiPs are capped with a dense bilayer of CTAB, which becomes increasingly sparse at the two tips of the BiPs, as evidenced in TEM images and shown schematically in Figure 2b,c. A similar scheme with a position-dependent CTAB barrier on gold nanorods was recently used to fabricate linear chains of these rods for SERS.[46] It will be shown here that this surface coating can also act as a barrier preventing the probe molecule (here Crystal Violet, CV) from adsorbing on the surface, except at the tips of the bipyramids, where the highest SERS enhancement factors (EFs) are expected.[50] As a result, we may expect that CV molecules adsorb only at hot-spots and, provided the adsorption efficiency is close to unity, every CV molecule in solution could therefore be detected at the single molecule level. Further information about sample preparation and detailed sample characterization are given in Sections S.I−S.III. of the Supporting Information, including TEM, dynamic light scattering (DLS), UV-vis extinction, and numerical modeling of their electromagnetic (EM) properties. The most important results are summarized in Figure 2.

SERS Experiments. In order to understand what happens in such a system for the SM-SERS properties, it is worth recalling the phenomenology of a standard SM-SERS experiment in a typical colloidal solution of partially aggregated Ag colloids. Using the bianalyte SERS method, one can show[16,22] that SM-SERS events can be observed with CV at 633 nm excitation at concentrations up to ≈10 nM CV, corresponding to ≈100 molecules per Ag particle. This is a reflection of the hot-spot localization effect, that is, the fact that hot-spots represent less than 1% of the available area for adsorption.[22−24] Under such conditions, typical maximum single molecule EFs (SMEFs) are of the order of 10^9-10^{10}, while average SERS EF (analytical EF, AEF[16]) are in the range $10^5 - 10^6$. The discrepancy of $\sim 10^4$ between SMEF and AEF arises partly from the hot-spot localization effect but also from the polydispersity of the colloidal solution (i.e., not all clusters are in resonance) and possibly from orientation averaging. In an ideal system where the situation in Figure 1III is achieved, polydispersity and hot-spot localization would be

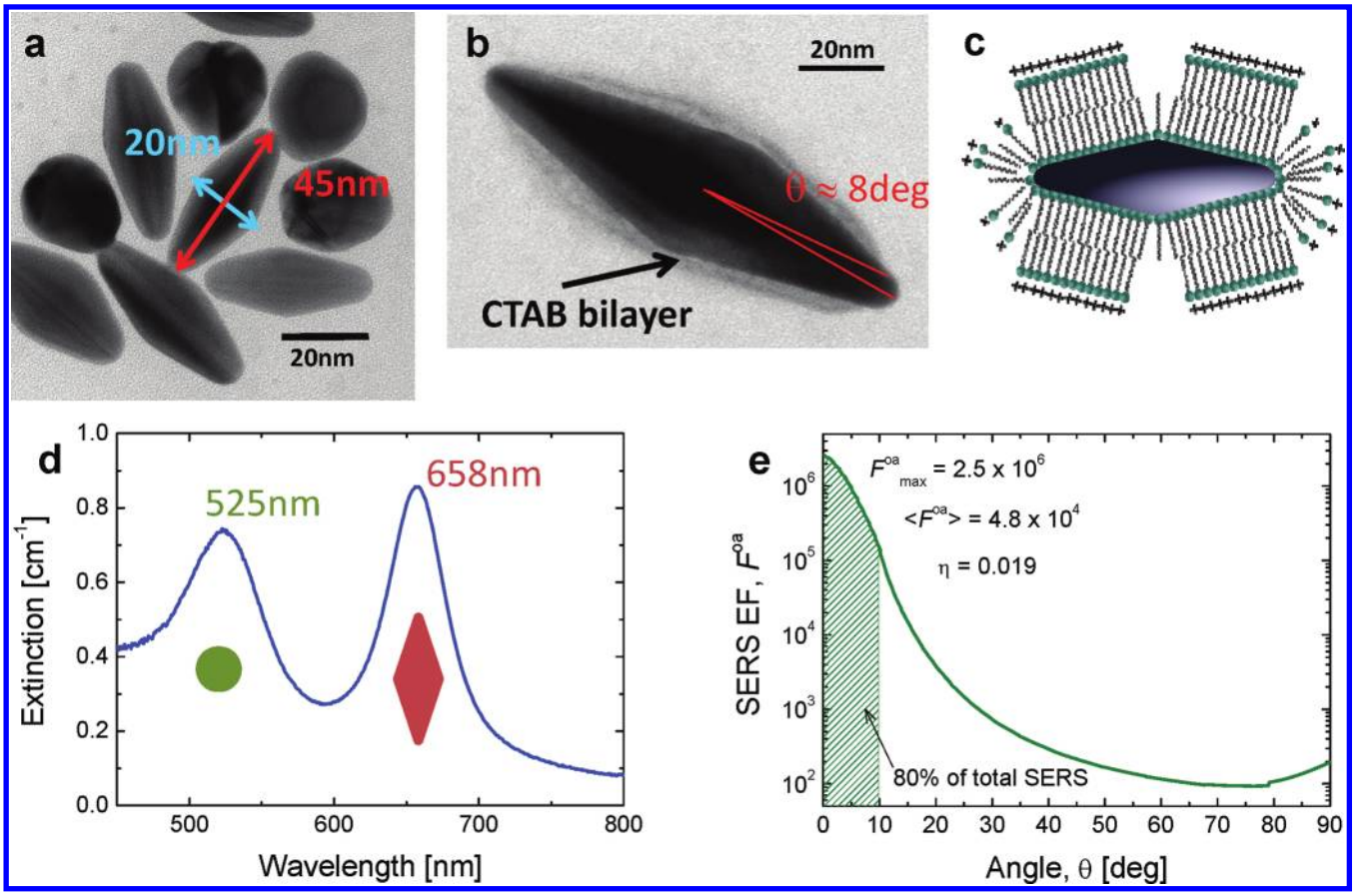

Figure 2. Colloidal solution characterization and theoretical modeling. (a) Wide-field TEM image showing the presence of both spherical and bipyramidal gold nanoparticles. The bipyramids appear very uniform in size and are typically 20 nm across and 45 nm high. (b) TEM image of CTAB-stabilized bipyramids synthesized using the same method as used in this work (note that these were obtained from a different batch where particle sizes are larger). The CTAB bilayer prevents adsorption of positively charged analytes like Crystal Violet on the surface except at the two tips where the SERS EF is largest; this is shown schematically in (c). (d) UV-vis extinction showing the relatively narrow localized surface plasmon resonance of the bipyramids around 658 nm, along with that of spheres at 525 nm. From these and electromagnetic calculations of extinction cross sections, the bipyramid concentration is estimated to be ~0.24 nM. (e) Calculations of the orientation-averaged (over incident polarizations) SERS enhancement factor distribution on the surface of the bipyramids. Eighty percent of the total SERS signal originates from a small area around the tip (4.4% of the total surface area). The predicted SM-SERS figure of merit (defined in the text) for random adsorption is $\eta = 0.019$ in the ideal monodisperse case. Only specific adsorption at the tip could lead to higher values as measured experimentally. See Supporting Information Figures S1 and S2 for further details.

avoided and this should result in a comparable value (except for possible orientation effects) for the maximum SMEF and the average AEF, that is, every analyte in solution experiences a SERS EF close to the maximum SMEF and is therefore detectable at the SM level if the latter is large enough. This observation provides an experimental methodology for demonstrating the actual realization of the situation in Figure 1III, which we follow here. To this end, it is useful to define a figure of merit for SM-SERS efficiency as η = AEF/SMEF. For the typical colloidal solutions discussed above, $\eta \approx 10^{-4}$, which may potentially be improved to 10^{-3} for a solution of monodisperse dimers. In fact, under the best reported controlled conditions of colloidal aggregates (in terms of size and gap dimensions), η of the order of $\sim 10^{-4}$ was measured.[44] However, if specific adsorption of every analyte in solution at the hot-spot is achieved, then this could theoretically reach values as high as $0.1 \leq \eta \leq 1$. Depending on the system under study, there may be physical limits to the maximum value of η, for example associated with orientation-averaging of the particle axis with respect to incident polarization or of the molecular orientation with respect to the local field polarization at the hot-spots (i.e., surface selection rules[S1,S2]). In the ideal case of $\eta = 1$, every analyte in solution is detected with exactly the same EF. Even in the best experimentally achievable cases of say $\eta \geq 0.1$, almost every analyte should be detectable at the single molecule level. We propose here to demonstrate the site-selective adsorption by measuring η, which requires a measurement of both the average and maximum single molecule SERS EFs. Such a methodology does not rely on uncertain concentration estimates (of either NPs or analytes) and should moreover be applicable to other SERS systems aiming for detection of every single target molecule, even beyond the hot-spot-selective adsorption approach demonstrated here.

The conditions under which SM-SERS may be observed are a convolution of a number of inter-related factors. For example, total surface area, hot-spot area, nanoparticle (NP) concentration, and analyte adsorption efficiency all affect the number of detectable (at a hot-spot) molecules per particle. Similarly, NP concentration, NP diffusion time in the scattering volume, and integration time affect the number of observed particles per event. It is because of this complexity that an independent experimental confirmation (as opposed to theoretical estimates) of SM-SERS is necessary, using for example the bianalyte SERS method.

dx.doi.org/10.1021/nl2030344 |Nano Lett. 2011, 11, 5013–5019

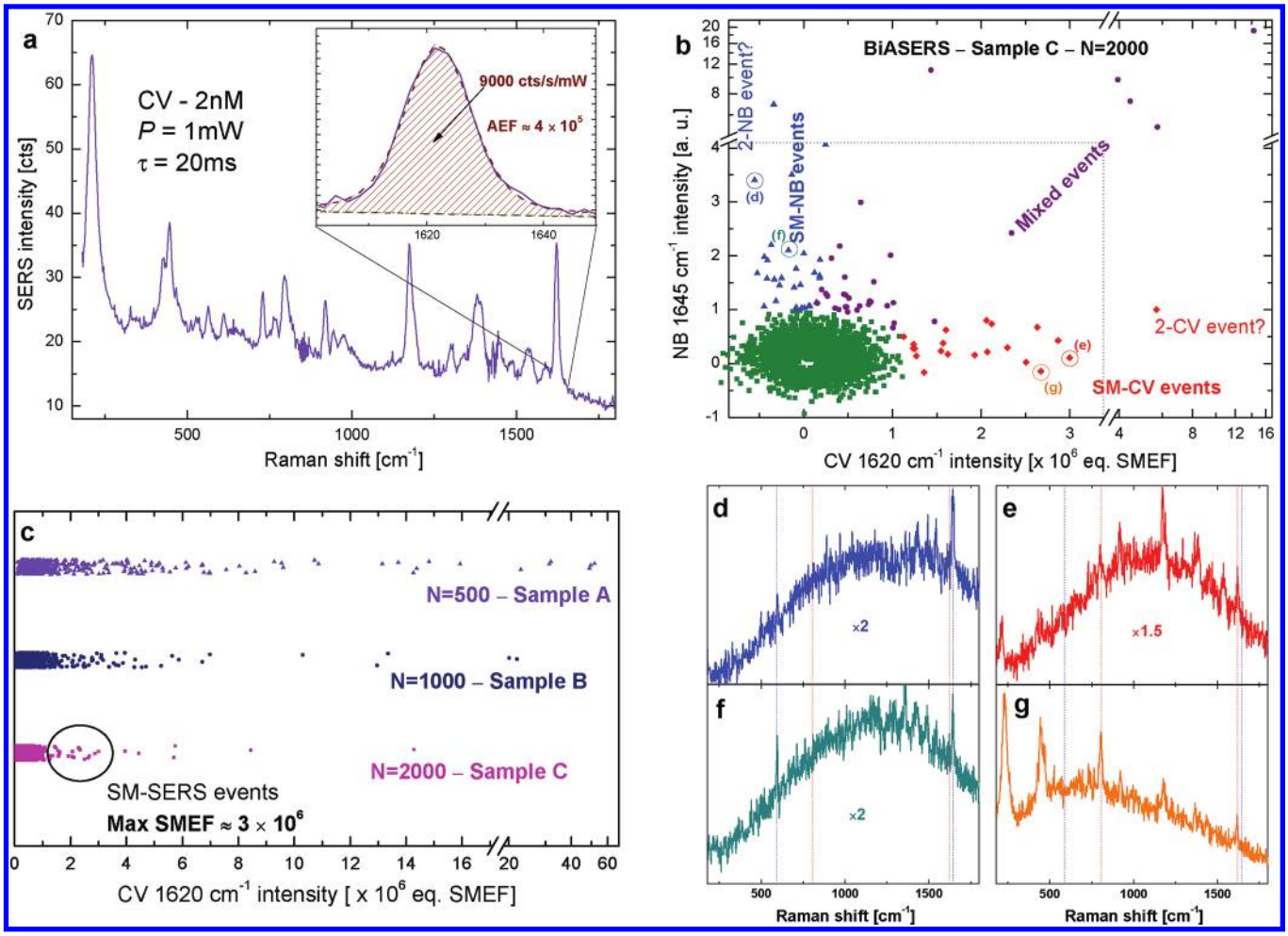

Figure 3. SERS experiments. (a) Average SERS spectrum for sample A (c_{CV} = 2 nM, c_{BiP} = 0.024 nM) obtained from 1000 individual spectra (integration time τ = 20 ms, taken at Δt = 94 ms intervals). The corresponding average SERS EF for the 1620 cm^{-1} mode of CV is 4×10^5. (b) Bianalyte SERS analysis showing a scatter plot of NB vs CV intensities for sample C (c_{CV} = 0.25 nM, c_{BiP} = 0.12 nM) for which the number of CV molecule per BiP particle is 40 times less than for sample A. Red (blue) events correspond to SM-SERS CV (NB) spectra. Purple events are mixed spectra. Green events are below the sensitivity of our analysis. CV intensities are expressed in equivalent SM-SERS EF, that is, it is the corresponding SM-SERS enhancement factor if the SERS signal originates from a single CV molecule. The statistics show that the single-molecule regime is achieved and that SM-SERS CV events occur with maximum SMEF of the order of 3×10^6. Also shown are representative SM-SERS spectra of NB (d,f) and CV (e,g). (c) Distributions of CV SERS intensities for decreasing number of CV molecules per hot-spot (HS) (sample A, 42 CV/HS, top; sample B, 4 CV/HS, middle; sample C, 1 CV/HS, bottom). *N* is the number of SERS events used for the statistics. The decrease in the maximum representative SERS EF shows that the single-molecule regime is not achieved until the concentrations are as low as those of sample C.

Because of uncertainties in preparing samples with accurate ultralow concentration, we first carried out measurements of average SERS EF on CV samples with intermediate concentrations (Sample A, with final concentrations of 2 nM CV and 0.024 nM BiP, that is, ×10 dilution of the starting colloidal solution). The results are summarized in Figure 3a. By varying the power, we first found the conditions under which the effect of photobleaching was negligible (see Supporting Information Table S.I) and deduced from the average SERS intensity an analytical SERS EF of ~4×10^5 for the 1620 cm^{-1} mode of CV in this sample. Thanks to the low colloid concentration in this sample, it is also interesting to note that we can observe the diffusion of individual bipyramids through our scattering volume (which has a Gaussian intensity profile with a waist diameter of $2w_0$ = 1.38 μm) over several consecutive spectra as discussed in the Supporting Information. From these and DLS measurements, the diffusion coefficient of the bipyramids is found to be $D \approx 13\ \mu m^2/s$, which corresponds for example to a rms displacement of 1.1 μm in 100 ms, or 2.5 μm in 500 ms. Integration times of 100 ms or lower therefore typically allow for the observation of a single bipyramid before it exits the scattering volume.

Bianalyte SERS Experiments. Bianalyte SERS experiments were carried out using Nile Blue (NB) as a bianalyte partner to CV. Given the low concentration of CV molecules per particle in sample A (30−80 depending on whether it adsorbs on spheres or not), the SM-SERS regime was here expected since at most one molecule would randomly adsorb at a hot-spot (whose area is only typically 1% of the total area). However, bianalyte experiments on sample with CV concentrations comparable to sample A failed to evidence SM-SERS spectra of CV. This gives us a first indication of the specific adsorption of CV at hot-spots. Interestingly, some NB single molecule SERS events could be observed, which could indicate that either NB does not adsorb specifically at the hot-spots, or that it does but with a much

dx.doi.org/10.1021/nl2030344 |*Nano Lett.* 2011, 11, 5013–5019

smaller adsorption efficiency than CV by a factor 10−20. In fact, the measured average EF for NB was about 10 times smaller than that of CV, which would therefore support the latter interpretation. In any case, this reduced adsorption efficiency affects the SM figure of merit η for NB and would complicate the analysis so we will therefore focus mostly on CV in the following, using only NB as a bianalyte partner with its concentration adjusted (to 10 times larger than CV) to account for the limited adsorption.

In order to probe further the SM-SERS regime for CV and determine the maximum SM-SERS EF in such conditions, bianalyte experiments at increasingly reduced numbers of molecules per particle were performed. In order to avoid problems associated with ultralow concentrations, the bipyramid concentrations were also increased. Two representative cases, samples B and C, are discussed here. As with sample A, a large number of SERS spectra were obtained under conditions that avoid photobleaching effects (incident power of 1 mW, integration time of 100 ms). Thanks to the Brownian motion of the nanoparticles, these events correspond to different bipyramids with different numbers of CV molecules adsorbed on them and at their hot-spots. The bianalyte SERS analysis of sample C is shown in Figure 3b. The nature of the maximum intensity events can be ascertained thanks to the presence of two analytes. We see that the first few strongest events in sample C are actually mixed events, where both NB and CV molecules were adsorbed at a HS. The majority of the strongest SM-SERS CV events correspond to SERS EF in the range $1.5-3 \times 10^6$. Occasional stronger events in Figure 3b can be attributed to events with 2 CV molecules. Similar observations are made for NB. Examples of SM-SERS spectra of CV and NB are shown in Figure 3d−g. It is interesting to note the change in relative intensities of peaks in either (d,f) for NB or (e,g) for CV. These reflect the small variations in the underlying localized surface plasmon (LSP) resonance from one particle to another, as previously observed in Ag colloids.[53,54] We also note the presence of the residual surface-enhanced fluorescence background as pointed out previously.[55] Similar bianalyte SERS results were obtained on sample B (with a 4× higher concentration of molecules per particle), except that a larger number of mixed events was obtained, indicating the transition from single-molecule to few-molecule regime.

A second type of analysis, based on the distribution of SERS intensities at each concentration, was also used to strengthen the conclusion. In the single molecule regime, the representative maximum intensities should not vary with concentration as they originate from a single CV molecule in optimum conditions (best location at a hot-spot, best BiP LSP resonance). The occurrence of maximum intensity events should however become less frequent as the CV concentration is reduced. This type of statistical analysis of SM-SERS has been discussed previously in detail.[56] The results, shown in Figure 3c, indeed confirm that sample A (with an estimated 42 CV/HS for specific adsorption) is far from being in the SM-SERS regime, and that only when going down to concentrations as low as 1 CV/HS (sample C) do we observe indication of SM-SERS.

Discussion and Conclusions. The SERS measurements suggest that, for the bipyramid/CV system under study, the SM-SERS figure of merit introduced earlier is $\eta \approx 0.13$, that is a factor of $\sim 10^3$ better than the commonly used Lee & Meisel Ag colloids. These BiP solutions therefore exhibit the remarkable property that the maximum SM-SERS EF is very close in magnitude to the average SERS EF for CV. This property can be traced back to the selective adsorption of the analyte at hot-spots where the SERS EF is maximum and the measurement of η provides a relatively general approach to demonstrate it experimentally. We note that the frequency of single-molecule events should also be increased in this case (Figure 1III) compared to conventional SMSERS with nonselective adsorption (Figure 1II). The experimental comparison between the two cases (ideally for the same SERS system) is however difficult in practice, and we believe that our approach of measuring η is much more versatile.

We also note that the maximum value of η in an ideal system is $\eta = 1$ and the remaining factor of 7−8 in our case compared to the ideal case can be attributed to a combination of factors: (i) the small polydispersity of the bipyramid solution may still result in small changes in resonance condition from one event to another, as observed in Figure 3d−g; (ii) incomplete adsorption of CV molecules in solution on the BiP NPs; (iii) varying molecular orientation with respect to local field polarization at the hot-spot (i.e., surface selection rules); (iv) the remaining SERS EF variation in the area at the BiP tip where adsorption is allowed (e.g., if the CV molecule is not exactly at the hot-spot, its SERS EF will be smaller than the maximum SERS EF). In fact, theoretical modeling suggests that this latter factor may reduce the maximum η to ∼0.34 in our case here, showing that it may be the dominant factor. Despite these remaining imperfections, it is clear that almost every CV molecule experiences a SERS EF close to the maximum value (by up to a factor of say 10, which is small by SM-SERS standards) and can therefore be detected provided the maximum SERS EF and the detection sensitivity are adequate. The detection limit in Figure 3b is not sufficient as it is a factor of ∼3 smaller than the maximum SERS EF. This is because the incident laser power was kept low to avoid the influence of photobleaching on the estimation of the SERS EF. If the SERS EF does not need to be determined, it is then possible to increase the incident power to 10 mW, which then allows the detection of every SERS CV molecule in solution at the single molecule level.

In closing, we briefly discuss possible improvements to the scheme demonstrated in this work. We first highlight again the fairly general applicability of both the chemical method of obtaining selective adsorption at hot-spots and the experimental approach to demonstrate its efficacy by estimating η. Both could equally be applied to other types of colloidal solutions or to fixed substrates such as those fabricated by nanolithography. The CTAB bilayer is a relatively easy approach that naturally favors adsorption at the positions of highest curvature on the nanoparticles, which are precisely those where EM hot-spots are expected. This may not however apply to gap-containing substrates, and the adsorption selectivity is also likely to be strongly analyte-dependent. Other barrier layers, possibly combined with selective chemical functionalization at hot-spots could be envisaged to overcome these problems. Moreover, the type of nanoparticles used as a proof-of-principle in this work are clearly not the ones sustaining the largest maximum SERS EF. It is likely that optimization of particle size and shape could result in maximum SERS EF in excess of 10^8, while conserving a high SM-SERS figure of merit of $\eta \approx 0.1$ when using a CTAB bilayer. This should in turn allow this method to be applied to other less resonant analytes with the ultimate goal being the detection of nonresonant analytes. With such potential improvements in mind, we believe that this study paves the way for highly controlled and reproducible routine detection of single molecules via SERS.

■ ASSOCIATED CONTENT

Supporting Information. Detailed procedures and results for the biypiramid synthesis, theoretical calculations of extinction and local fields, sample preparation and characterization, and estimation of SERS enhancement factors. This material is available free of charge via the Internet at http://pubs.acs.org.

■ AUTHOR INFORMATION

Corresponding Author

*E-mail: (E.C.L.R.) eric.leru@vuw.ac.nz; (J.G.) johan.grand@univ-paris-diderot.fr.

■ ACKNOWLEDGMENT

E.C.L.R. is indebted to the Royal Society of New Zealand for support through a Marsden Grant and Rutherford Discovery Fellowship.

■ REFERENCES

(1) Nie, S.; Emory, S. R. Probing single molecules and single nanoparticles by surface-enhanced Raman scattering. *Science* **1997**, *275*, 1102–1106.

(2) Kneipp, K.; Wang, Y.; Kneipp, H.; Perelman, L. T.; Itzkan, I.; Dasari, R. R.; Feld, M. S. Single molecule detection using surface-enhanced Raman scattering (SERS). *Phys. Rev. Lett.* **1997**, *78*, 1667–1670.

(3) Le Ru, E. C.; Etchegoin, P. G. *Principles of Surface Enhanced Raman Spectroscopy and Related Plasmonic Effects*; Elsevier: Amsterdam, 2009.

(4) Aroca, R. F. *Surface-Enhanced Vibrational Spectroscopy*; John Wiley & Sons: Chichester, 2006.

(5) Campion, A.; Kambhampati, P. Surface-enhanced Raman scattering. *Chem. Soc. Rev.* **1998**, *27*, 241–250.

(6) Jiang, J.; Bosnick, K.; Maillard, M.; Brus, L. Single molecule Raman spectroscopy at the junctions of large Ag nanocrystals. *J. Phys. Chem. B* **2003**, *107*, 9964–9972.

(7) Habuchi, S.; Cotlet, M.; Gronheid, R.; Dirix, G.; Michiels, J.; Vanderleyden, J.; De Schryver, F. C.; Hofkens, J. Single-molecule surface enhanced resonance Raman spectroscopy of the enhanced green fluorescent protein. *J. Am. Chem. Soc.* **2003**, *125*, 8446–8447.

(8) Jackson, J. B.; Westcott, S. L.; Hirsch, L. R.; West, J. L.; Halas, N. J. Controlling the surface enhanced Raman effect via the nanoshell geometry. *Appl. Phys. Lett.* **2003**, *82*, 257–259.

(9) Lee, S. J.; Guan, Z.; Xu, H.; Moskovits, M. Surface-enhanced Raman spectroscopy and nano-geometry: the plasmonic origin of SERS. *J. Phys. Chem. C* **2007**, *111*, 17985–17988.

(10) Stranahan, S. M.; Willets, K. A. Super-resolution Optical Imaging of Single-Molecule SERS Hot Spots. *Nano Lett.* **2010**, *10*, 3777–3784.

(11) Li, J. F.; Huang, Y. F.; Ding, Y.; Yang, Z. L.; Li, S. B.; Zhou, X. S.; Fan, F. R.; Zhang, W.; Zhou, Z. Y.; Wu, D. Y.; Ren, B.; Wang, Z. L.; Tian, Z. Q. Shell-isolated nanoparticle-enhanced Raman spectroscopy. *Nature* **2010**, *464*, 392–395.

(12) Moerner, W. E.; Kador, L. Optical detection and spectroscopy of single molecules in a solid. *Phys. Rev. Lett.* **1989**, *62*, 2535–2538.

(13) Ambrose, W. P.; Moerner, W. E. Fluorescence spectroscopy and spectral diffusion of single impurity molecules in a crystal. *Nature* **1991**, *349*, 225–227.

(14) Ambrose, W. P.; Goodwin, P. M.; Jett, J. H.; Van Orden, A.; Werner, J. H.; Keller, R. A. Single Molecule Fluorescence Spectroscopy at Ambient Temperature. *Chem. Rev.* **1999**, *99*, 2929–2956.

(15) Xu, H.; Bjerneld, E. J.; Käll, M.; Börjesson, L. Spectroscopy of single hemoglobin molecules by surface enhanced Raman scattering. *Phys. Rev. Lett.* **1999**, *83*, 4357–4360.

(16) Le Ru, E. C.; Blackie, E.; Meyer, M.; Etchegoin, P. G. Surface Enhanced Raman Scattering enhancement factors: a comprehensive study. *J. Phys. Chem. C* **2007**, *111*, 13794–13803.

(17) Xu, H.; Aizpurua, J.; Kall, M.; Apell, P. Electromagnetic contributions to single-molecule sensitivity in surface-enhanced Raman scattering. *Phys. Rev. E* **2000**, *62*, 4318–4324.

(18) Schatz, G. C.; Young, M. A.; Van Duyne, R. P. Electromagnetic mechanism of SERS. *Top. Appl. Phys.* **2006**, *103*, 19–46.

(19) Blackie, E. J.; Le Ru, E. C.; Etchegoin, P. G. Single molecule surface-enhanced Raman spectroscopy of non-resonant molecules. *J. Am. Chem. Soc.* **2009**, *131*, 14466–14472.

(20) Gu, G. H.; Suh, J. S. Minimum Enhancement of Surface-Enhanced Raman Scattering for Single-Molecule Detections. *J. Phys. Chem. A* **2009**, *113*, 8529–8532.

(21) Etchegoin, P. G.; Le Ru, E. C. A perspective on single molecule SERS: Current status and future challenges. *Phys. Chem. Chem. Phys.* **2008**, *10*, 6079–6089.

(22) Le Ru, E. C.; Meyer, M.; Etchegoin, P. G. Proof of Single-Molecule Sensitivity in Surface Enhanced Raman Scattering (SERS) by Means of a Two-Analyte Technique. *J. Phys. Chem. B* **2006**, *110*, 1944–1948.

(23) Le Ru, E. C.; Etchegoin, P. G.; Meyer, M. Enhancement factor distribution around a single SERS hot-spot and its relation to single molecule detection. *J. Chem. Phys.* **2006**, *125*, 204701.

(24) Fang, Y.; Seong, N.-H.; Dlott, D. D. Measurement of the distribution of site enhancements in surface-enhanced Raman scattering. *Science* **2008**, *321*, 388–391.

(25) Dieringer, J. A.; Lettan, R. B., II; Scheidt, K. A.; Van Duyne, R. P. A frequency domain existence proof of single-molecule surface-enhanced Raman Spectroscopy. *J. Am. Chem. Soc.* **2007**, *129*, 16249–16256.

(26) Kleinman, S. L.; Ringe, E.; Valley, N.; Wustholz, K. L.; Phillips, E.; Scheidt, K. A.; Schatz, G. C.; Van Duyne, R. P. Single-Molecule Surface-Enhanced Raman Spectroscopy of Crystal Violet Isotopologues: Theory and Experiment. *J. Am. Chem. Soc.* **2011**, *133*, 4115–4122.

(27) Goulet, P. J. G.; Aroca, R. F. Distinguishing individual vibrational fingerprints: Single-molecule surface-enhanced resonance Raman scattering from one-to-one binary mixtures in Langmuir-Blodgett monolayers. *Anal. Chem.* **2007**, *79*, 2728–2734.

(28) Sawai, Y.; Takimoto, B.; Nabika, H.; Ajito, K.; Murakoshi, K. Observation of a Small Number of Molecules at a Metal Nanogap Arrayed on a Solid Surface Using Surface-Enhanced Raman Scattering. *J. Am. Chem. Soc.* **2007**, *129*, 1658–1662.

(29) Cortes, E.; Etchegoin, P. G.; Le Ru, E. C.; Fainstein, A.; Vela, M. E.; Salvarezza, R. C. Monitoring the Electrochemistry of Single Molecules by Surface-Enhanced Raman Spectroscopy. *J. Am. Chem. Soc.* **2010**, *132*, 18034–18037.

(30) Dieringer, J. A.; Wustholz, K. L.; Masiello, D. J.; Camden, J. P.; Kleinman, S. L.; Schatz, G. C.; Van Duyne, R. P. Surface-Enhanced Raman Excitation Spectroscopy of a Single Rhodamine 6G Molecule. *J. Am. Chem. Soc.* **2009**, *131*, 849–854.

(31) Ward, D. R.; Halas, N. J.; Ciszek, J. W.; Tour, J. M.; Wu, Y.; Nordlander, P.; Natelson, D. Simultaneous Measurements of Electronic Conduction and Raman Response in Molecular Junctions. *Nano Lett.* **2008**, *8*, 919–924.

(32) Ward, D. R.; Corley, D. A.; Tour, J. M.; Natelson, D. Vibrational and electronic heating in nanoscale junctions. *Nat. Nanotechnol.* **2010**, *6*, 33–38.

(33) Etchegoin, P. G.; Le Ru, E. C. Resolving Single Molecules in Surface-Enhanced Raman Scattering within the Inhomogeneous Broadening of Raman Peaks. *Anal. Chem.* **2010**, *82*, 2888–2892.

(34) Pettinger, B.; Ren, B.; Picardi, G.; Schuster, R.; Ertl, G. Nanoscale Probing of Adsorbed Species by Tip-Enhanced Raman Spectroscopy. *Phys. Rev. Lett.* **2004**, *92*, 096101.

(35) Pettinger, B. Single-molecule surface- and tip-enhanced Raman spectroscopy. *Mol. Phys.* **2010**, *108*, 2039–2059.

(36) Liu, Z.; Ding, S.-Y.; Chen, Z.-B.; Wang, X.; Tian, J.-H.; Anema, J. R.; Zhou, X.-S.; Wu, D.-Y.; Mao, B.-W.; Xu, X.; Ren, B.; Tian, Z.-Q.

Revealing the molecular structure of single-molecule junctions in different conductance states by fishing-mode tip-enhanced Raman spectroscopy. *Nat. Commun.* **2011**, *2*, 305.

(37) Alvarez-Puebla, R. A.; Contreras-Caceres, R.; Pastoriza-Santos, I.; Perez-Juste, J.; Liz-Marzan, L. M. Au@pNIPAM Colloids as Molecular Traps for Surface-Enhanced, Spectroscopic, Ultra-Sensitive Analysis. *Angew. Chem., Int. Ed.* **2009**, *48*, 138–143.

(38) Chen, G.; Wang, Y.; Yang, M.; Xu, J.; Goh, S. J.; Pan, M.; Chen, H. Measuring Ensemble-Averaged Surface-Enhanced Raman Scattering in the Hotspots of Colloidal Nanoparticle Dimers and Trimers. *J. Am. Chem. Soc.* **2010**, *132*, 3644–3645.

(39) Lim, D.-K.; Jeon, K.-S.; Kim, H. M.; Nam, J.-M.; Suh, Y. D. Nanogap-engineerable Raman-active nanodumbbells for single-molecule detection. *Nat. Mater.* **2010**, *9*, 60–67.

(40) Wang, H.; Levin, C. S.; Halas, N. J. Nanosphere Arrays with Controlled Sub-10-nm Gaps as Surface-Enhanced Raman Spectroscopy Substrates. *J. Am. Chem. Soc.* **2005**, *127*, 14992–14993.

(41) Vlckova, B.; Moskovits, M.; Pavel, I.; Siskova, K.; Sladkova, M.; Slouf, M. Single-molecule surface-enhanced Raman spectroscopy from a molecularly-bridged silver nanoparticle dimer. *Chem. Phys. Lett.* **2008**, *455*, 131–134.

(42) Graham, D.; Thompson, D. G.; Smith, W. E.; Faulds, K. Control of enhanced Raman scattering using a DNA-based assembly process of dye-coded nanoparticles. *Nat. Nanotechnol.* **2008**, *3*, 548–551.

(43) Li, W.; Camargo, P. H. C.; Lu, X.; Xia, Y. Dimers of Silver Nanospheres: Facile Synthesis and Their Use as Hot Spots for Surface-Enhanced Raman Scattering. *Nano Lett.* **2009**, *9*, 485–490.

(44) Taylor, R. W.; Lee, T.-C.; Scherman, O. A.; Esteban, R.; Aizpurua, J.; Huang, F. M.; Baumberg, J. J.; Mahajan, S. Precise Subnanometer Plasmonic Junctions for SERS within Gold Nanoparticle Assemblies Using Cucurbit[n]uril "Glue. *ACS Nano* **2011**, *5*, 3878–3887.

(45) Lim, D.-K.; Jeon, K.-S.; Hwang, J.-H.; Kim, H.; Kwon, S.; Suh, Y. D.; Nam, J.-M. Highly uniform and reproducible surface-enhanced Raman scattering from DNA-tailorable nanoparticles with 1-nm interior gap. *Nat. Nanotechnol.* **2011**, *6*, 452−460.

(46) Lee, A.; Andrade, G. F. S.; Ahmed, A.; Souza, M. L.; Coombs, N.; Tumarkin, E.; Liu, K.; Gordon, R.; Brolo, A. G.; Kumacheva, E. Probing Dynamic Generation of Hot-Spots in Self-Assembled Chains of Gold Nanorods by Surface-Enhanced Raman Scattering. *J. Am. Chem. Soc.* **2011**, *133*, 7563–7570.

(47) Chen, T.; Wang, H.; Chen, G.; Wang, Y.; Feng, Y.; Teo, W. S.; Wu, T.; Chen, H. Hotspot-Induced Transformation of Surface-Enhanced Raman Scattering Fingerprints. *ACS Nano* **2010**, *4*, 3087–3094.

(48) Chen, T.; Du, C.; Tan, L. H.; Shen, Z.; Chen, H. Site-selective localization of analytes on gold nanorod surface for investigating field enhancement distribution in surface-enhanced Raman scattering. *Nanoscale* **2011**, *3*, 1575–1581.

(49) Liu, M. Z.; Guyot-Sionnest, P. J. Mechanism of silver(I)-assisted growth of gold nanorods and bipyramids. *J. Phys. Chem. B* **2005**, *109*, 22192–22200.

(50) Liu, M.; Guyot-Sionnest, P.; Lee, T.-W.; Gray, S. K. Optical properties of rodlike and bipyramidal gold nanoparticles from three-dimensional computations. *Phys. Rev. B* **2007**, *76*, 235428.

(51) Moskovits, M. Surface selection rules. *J. Chem. Phys.* **1982**, *77*, 4408–4416.

(52) Le Ru, E. C.; Meyer, S. A.; Artur, C.; Etchegoin, P. G.; Grand, J.; Lang, P.; Maurel, F. Experimental demonstration of surface selection rules for SERS on flat metallic surfaces. *Chem. Commun.* **2011**, *47*, 3903–3905.

(53) Buchanan, S.; Le Ru, E. C.; Etchegoin, P. G. Plasmon-dispersion corrections and constraints for surface selection rules of single molecule SERS spectra. *Phys. Chem. Chem. Phys.* **2009**, *11*, 7406–7411.

(54) Yoshida, K.-i.; Itoh, T.; Biju, V.; Ishikawa, M.; Ozaki, Y. Experimental evaluation of the twofold electromagnetic enhancement theory of surface-enhanced resonance Raman scattering. *Phys. Rev. B* **2009**, *79*, 085419.

(55) Galloway, C. M.; Etchegoin, P. G.; Le Ru, E. C. Ultrafast nonradiative decay rates on metallic surfaces by comparing surface-enhanced Raman and fluorescence signals of single molecules. *Phys. Rev. Lett.* **2009**, *103*, 063003.

(56) Bohn, J. E.; Le Ru, E. C.; Etchegoin, P. G. A Statistical Criterion for Evaluating the Single-Molecule Character of SERS Signals. *J. Phys. Chem. C* **2010**, *114*, 7330–7335.

Supplementary information for "A scheme for detecting every single target molecule with surface-enhanced Raman spectroscopy"

S.I. BIPYRAMID SYNTHESIS

The gold bipyramids (BiPs) were synthesized by a seed mediated protocol according to the method developed by Liu and Guyot-Sionnest [1].

Seed solution: 20 mL of 0.125 mM $HAuCl_4$ solution was prepared by dissolving 100 μL of 25 mM $HAuCl_4$ in 20 mL DI water. Then, 200 μL of 25 mM trisodium citrate were added to give a final citrate concentration of 0.25 mM. Finally, 300 μL of freshly prepared 10 mM $NaBH_4$ were quickly injected under vigorous stirring.

Growth solution: The reaction was performed in a water bath set up at 30°C. To 10 mL of 100 mM cethylmethylammonium bromide (CTAB) solution were added 200 μL of 25 mM $HAuCl_4$ stock along with 100 μL of 10 mM $AgNO_3$. The solution was then acidified with 200 μL of 1 M HCl. Next 80 μL of 100 mM ascorbic acid were added. The subsequent reduction of Au^{III} to Au^{I} was evidenced by a complete discoloration of the reaction mixture. The growth was initiated by injecting 300 μL of seed solution (this can be changed to modify the final BiP size if needed) and the solution was left to react under gentle stirring for 90 minutes. Finally, the bipyramids were isolated from the reaction medium by centrifugation at 6000 rpm for 5 minutes. The nanoparticles were redispersed in 10 mL of DI water and precipitated again by centrifugation to remove excess CTAB. The washing process was repeated once and the nanoparticles were eventually redispersed in DI water.

The as-prepared solution was then diluted by a factor ≈ 10 before all further sample preparation. This diluted solution is what we will refer as the starting solution.

S.II. THEORETICAL CALCULATIONS

Theoretical calculations were performed in a model system to characterize the extinction spectra of the bipyramids and the distribution of EM field enhancements on their surface. The half-bipyramids were approximated as tip-rounded right-circular cones with basis diameter of 20 nm and height of 22.5 nm (i.e. 45 nm total height for the bipyramid). The tip was rounded using a spheroidal cap geometry. The conical and spheroidal geometries are joined in such a way that the resulting surface and its first derivative (i.e. the normal to the surface) are both continuous. This is represented schematically in Fig. **S1**(A). As shown in Fig. **S1**(B), these parameters are consistent with those measured by electron microscopy and were further tuned to match the experimental LSP resonance at 658 nm. The gold particle was assumed to be embedded in water (relative dielectric function $\epsilon_M = 1.77$) and the wavelength-dependent dielectric function of gold was obtained from an analytical fit to experimental data as given in Ref. [2]. For simplicity, we have omitted the presence of the CTAB bilayer in these calculations, since it only had a minor effect on the results. For example, when embedding the bipyramid in a CTAB layer represented by a shell of refractive index $n = 1.4$ with a varying thickness of 4 nm on the side and zero at the tip, the extinction maximum was redshifted by only ≈ 4 nm while its maximum changed by only $\approx 4\%$.

Calculation of extinction spectra

Given the relatively small size of the bipyramids, the electrostatic approximation (ESA) provides a good approximation to the exact EM problem. Calculations were therefore performed in the ESA via finite-element modeling using the software COMSOL 4.1. A 3D model was used to calculate the orientation-averaged (using 21 incident field polarizations) extinction cross-section of the bipyramids. As shown in Fig. **S1**(C), this was found to be almost identical to the extinction cross-section with polarization along the bipyramid axis, except for a factor 1/3 due to orientation averaging (which is expected for a dipolar resonance and comes from the averaging of a $\cos^2$ factor). The latter case of excitation along the axis can in fact be modeled much more efficiently as a 2D axisymmetric model, and therefore provides an easy way to check the accuracy of the more demanding 3D calculations. The predicted extinction spectrum (Fig. **S1**(C)) is in good agreement with the experimental extinction spectra obtained from UV-Vis extinction and therefore provides a way of inferring the particle concentration in solution (see below). The broader experimental resonance (53 nm FWHM vs 31 nm for predictions) reflects the small dispersity in the shape and size of the bipyramids.

Calculation of local field enhancements

Using an excitation wavelength of $\lambda_L = 633$ nm (with a polarization along the bipyramid axis), and a Raman wavelength of $\lambda_R = 705$ nm (corresponding to the 1620 cm^{-1} mode of CV), we also computed in the ESA the local field intensity enhancement factors (LFIEF), $M_{\mathrm{Loc}} = |E|^2/|E_0|^2$, and the SERS EFs in the $|E|^4$-approximation, $F = M_{\mathrm{Loc}}(\lambda_L)M_{\mathrm{Loc}}(\lambda_R)$ at all positions

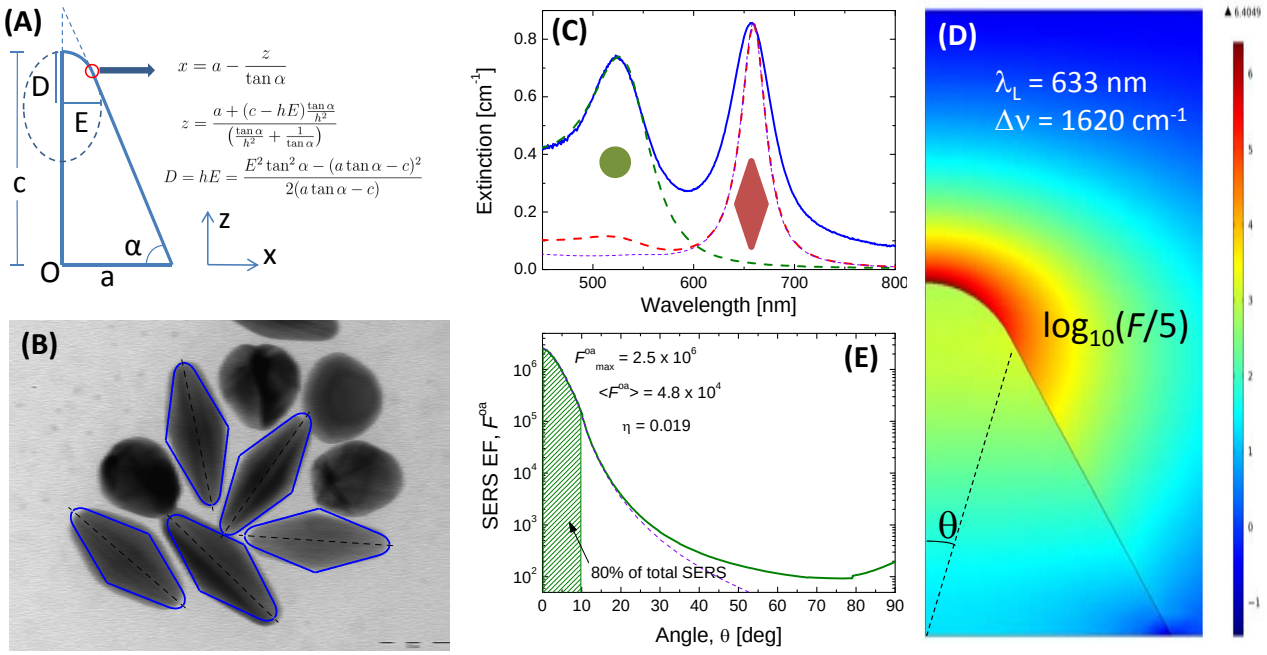

Supplementary Figure S1: (A) Geometry used for theoretical calculations of the optical properties of the bipyramids. The structure has symmetry of revolution around the z axis and consists of a truncated cone with a prolate spheroidal cap. The formulae given above ensure continuity of the surface and its first derivative (normal). (B) The shape in (A) with same dimensions is superimposed in blue onto TEM images of the bipyramid sample, showing the good agreement between the structure chosen for modelling and the real bipyramids. (C) Experimental (solid lines) and predicted (dotted lines) extinction spectra. Predictions for spheres (green) were obtained from Mie theory for a 12.5 nm radius gold sphere in water. The orientation-averaged extinction for the bipyramid (red) is also compared with the approximation obtained from taking 1/3 of the extinction with incident polarization along the main axis (purple). (D) Predicted spatial distribution of the SERS enhancement factor, F, on the surface for incident polarization along the main axis, computed in the $|E|^4$-approximation for laser excitation at $\lambda_L = 633$ nm and Raman wavelength of $\lambda_R = 705$ nm (i.e. Raman shift of 1620 cm^{-1}). Note that we show here $F/5$, which provides a good approximation, to orientation-averaged SERS EF, F^{oa} (averaged over bipyramid orientation). (E) Orientation-averaged SERS EF, F^{oa}, on the bipyramid surface as a function of co-latitude angle θ. The dashed area contributes to 80% of the total SERS signal but correspond to only 4.4% of its total surface area. Also shown as a dashed purple line is $F/5$, showing that $F^{\mathrm{oa}} \approx F/5$ except far from the tips, where the SERS EF is lowest.

on the bipyramid surface. The results of such calculations are shown in Fig. **S1**(D-E). Because the rotational diffusion time of the bipyramids is expected to be much faster than typical integration times in our SERS experiment, we consider the orientation-averaged (of the bipyramid axis with respect to incident polarization) SERS EF, F^{oa}. This orientation-averaged SERS EF could also have been inferred from the SERS EF for incident polarization along the main axis F^0 as $F^{\mathrm{oa}} = F^0/5$. This reflects, as for the extinction, the dipolar nature of the main resonance at 658 nm (the factor 1/5 comes from the average of a $\cos^4$ factor).

A maximum SERS EF of $F^{\mathrm{oa}}_{\mathrm{max}} = 2.5 \times 10^6$ (in agreement with experimental measurements) is predicted and occurs, as expected, at the tip. The magnitude of the SERS EF then drops significantly when moving away from the tip, because of the *hot-spot localization effect*. This effect manifests itself in a number of ways:

- the SERS EF drops by a factor of 2 at a distance (arc-length) of 1.7 nm only from the tip.
- Assuming random adsorption of molecules, the area around the tip that contributes to 80% (50%) of the total SERS signal is only 4.4% (1.6%) of the total surface area of the bipyramid.
- The surface-averaged SERS EF is only $\langle F^{\mathrm{oa}}\rangle = 4.8 \times 10^4$.

We can therefore deduce a theoretical optimum single molecule figure of merit (defined in main paper) for these bipyramids of $\eta = \langle F^{\mathrm{oa}}\rangle / F^{\mathrm{oa}}_{\mathrm{max}} = 0.019$ (assuming random adsorption). In reality, polydispersity and the fact that CV would also adsorb on the spheres would bring this figure further down.

In order to explain the high figure of merit observed experimentally, we must therefore assume specific adsorption of the analyte at the tip of the bipyramids. For the sake of argument, if we for example assume that CV may only adsorb within 4 nm (arclength along the surface) of the tip (as suggested in the TEM images showing the CTAB bilayer), then, the average SERS EF increases to 8.7×10^5, and the SM figure of merit to $\eta = 0.34$. The

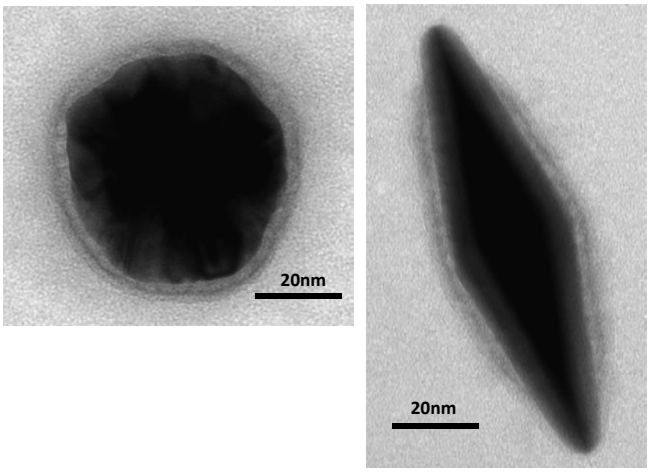

Supplementary Figure S2: TEM images of CTAB-stabilized gold nanoparticles synthesized using the same method as used in this work (note that these were obtained from a different solution where particle sizes are larger than the ones studied here). A CTAB bilayer of $\approx 4\,\mathrm{nm}$ is seen around both the spheres and the bipyramids, but does not cover the tips of the latter.

fact that η is not ≈ 1 still reflects the fact that there remains a non-negligible SERS EF distribution in the area accessible to molecular adsorption ($\approx 40\,\mathrm{nm}^2$ in this example). Indeed, the surface SERS EF 4 nm (arclength along the surface) away from the tip is 3×10^5, i.e. a factor of 10 smaller than at the top. This nevertheless represents a dramatic improvement in η compared to the random-adsorption case.

S.III. BIPYRAMID SOLUTION CHARACTERIZATION AND SAMPLE PREPARATION

TEM measurements

Coating with a polyoxometalate contrast agent for TEM imaging: In order to localise low contrast CTAB molecules onto bipyramids, we coated their surface with an electron rich staining agent belonging to the polyoxometalate (POM) family. POMs consist of transition metal oxyanions linked together in a 3D network by bridging oxygen atoms. Because they are electron dense, they have been commonly used as negative stain for imaging of biological samples by TEM. Here we used the Dawson type hexa -anionic $P_2W_{18}O_{62}^{6-}$ (POW) POM. Because of its polyanionic nature, it can electrostatically bind to the positively charged head of the outer CTAB layer around the bipyramids. The staining was done as follows. 200 μL of purified BiP solution whose extinction maximum had been adjusted to roughly 1 were mixed for 1 minute with 30 μL of a 1 mM POW solution. The mixture was dropcasted onto TEM micro-grids and imaged on a JEOL-100CX II microscope operating at 100kV.

Structural properties: The structural properties were obtained from TEM measurements such as those shown in Fig. 2a of the main text and Fig. **S1**(B). From these, it is seen that the colloidal solution contains both bipyramidal and spherical gold nanoparticles in a ratio of approximately 1:2. The spherical particles have a diameter of the order of 25 nm. The bipyramids have an hexagonal base and are on average 20 nm across and 45 nm high. Aggregates are observed in some of these images but are believed to be the result of the preparation of the sample for microscopy measurements. There is no indication of the presence of aggregates in the extinction spectrum (Fig. **S1**(C)) nor in the time dependence of the SERS measurements (see Fig. **S4** later). In fact, if the SERS signals originated only from a small number of aggregates, then a large number of analytes adsorbed on the non-aggregated BiPs would not be observable. This would result in a much smaller value for the single molecule figure of merit (η, defined in the text) than measured.

CTAB bilayer: TEM images were also obtained from a bipyramid solution in order to image the CTAB bilayer. The resulting images for a representative sphere and bipyramid are shown in Fig. **S2**. TEM images of the nanospheres display heavily contrasted gold cores surrounded by lighter contrasted CTAB shells, the latter being capped with a thin layer of medium contrast POW. The width of the CTAB layer is estimated to be 4nm from the distance between the gold surface and the POW molecules. This thickness matches what is expected for a lipidic bilayer structure. TEM images of bipyramids display similar features to that of spheres except for the distribution of the organic shell. The POW layer on top of the CTAB only appears on the large sidewall facets and not on the tips. This shows that the surfactant bilayer is broken at the tips, rendering the tips more denuded than the facets and therefore more likely to be accessed by the analyte. From these images, we can estimate the uncoated area at the tip to be of the order of 5% of the total surface area.

Diffusion coefficient from Dynamic Light Scattering

The diffusion coefficient of the bipyramid nanoparticles (appropriately diluted) was measured via dynamic light scattering (DLS) [3, 4] at a temperature of 25°C using 633 nm excitation at a scattering angle of 173°. The measured autocorrelation function along with a bi-exponential fit are shown in Fig. **S3**. We did not attempt to fit a more complicated multi-exponential to the data as we are here only after the order of magnitude of the diffusion coefficient (the relevance of the parameters obtained from a multi-exponential fit to the data in Fig. **S3** would be questionable anyway). The fast initial decay is always

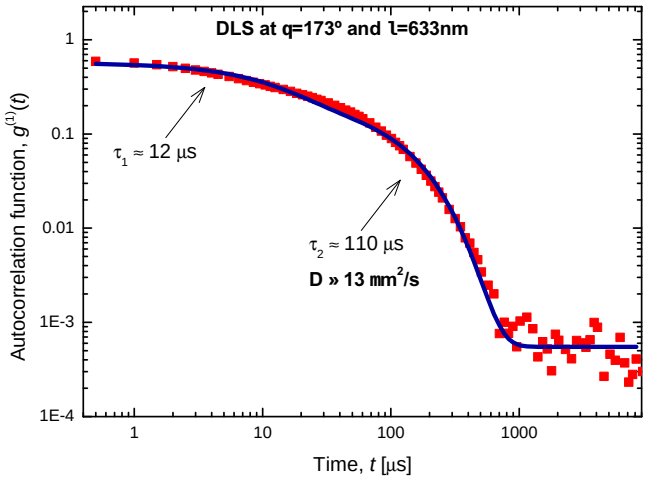

Supplementary Figure S3: Data from dynamic light scattering of the bipyramid solution at 633 nm excitation and a scattering angle of 173°. The first order normalized time autocorrelation function is shown (symbols) along with bi-exponential fit (line). The longer time constant is attributed to the diffusion of the nanoparticles and correspond to an approximate diffusion coefficient of $D = 13\,\mu\text{m}^2/\text{s}$.

observed in metallic colloids and is related to the non-zero optical absorption of the nano-particles. The longer time constant is associated with diffusion of the nanoparticles in solution and correspond to a diffusion coefficient of $D = 13\,\mu\text{m}^2/\text{s}$. We cannot in this experiment resolve the difference between the spheres and the bipyramids, but this measurement nevertheless provides us with a rough estimate of the diffusion coefficient, which is consistent with the time dependence of the SERS intensities as discussed in Sec. S.IV.

Nanoparticle concentrations

The concentration of each type of nanoparticle in solution can, to some extent, be estimated from the UV-Vis extinction measurement of Fig. **S1**(C):

- For the sphere first, Mie theory predicts for a 25 nm gold sphere in water a localized surface plasmon (LSP) resonance at 526 nm and an extinction coefficient [5] at resonance of $Q_{\text{ext}} = 1.54$, corresponding to a (decadic) molar extinction coefficient of $2.0 \times 10^9\,\text{cm}^{-1}\,\text{M}^{-1}$. The measured extinction for the spheres at resonance is $0.64\,\text{cm}^{-1}$ (the solution extinction is $0.75\,\text{cm}^{-1}$, but as shown in Fig. **S1**(C), about 15% originates from the BiP extinction).This corresponds to a sphere concentration of 0.32 nM or 0.19 NP/μm^3 in the starting solution.

- For the bipyramids, the theoretical extinction coefficient at resonance was estimated from the calculations presented in Sec. S.II. At the predicted LSP resonance at 658 nm, the absorption cross-section (approximately equal to extinction for such small particles) is $1.37 \times 10^{-11}\,\text{cm}^2$ after orientation averaging and correction for the broader resonance observed experimentally (the measured LSP resonance of the bipyramids is 1.7 times wider than predicted (53 nm FWHM compared to 31 nm). This corresponds to a predicted (decadic) molar extinction coefficient of $3.6 \times 10^9\,\text{cm}^{-1}\,\text{M}^{-1}$. Moreover, the measured maximum extinction for the bipyramids at resonance is $0.86\,\text{cm}^{-1}$ (at 658 nm), which therefore corresponds to a bipyramid concentration of 0.24 nM or 0.14 NP/μm^3 in the starting solution.

The sphere and bipyramids concentrations differ therefore by an approximate 1.4:1 ratio, as also observed qualitatively in microscopy images (the predicted ratio depends strongly on the size chosen for the sphere and is therefore not accurate).

Number of molecules per particles

The surface area (available for non-specific adsorption) of each particle can also be calculated: it is $\approx 2000\,\text{nm}^2$ for the spheres and $\approx 1800\,\text{nm}^2$ for the bipyramids. Using the concentrations given above, we deduce that random adsorption would result with approximate 60%:40% relative probability of adsorption on spheres and bipyramids. Therefore, a concentration of 0.6 nM of analyte in solution would result (with random adsorption) in $\approx$ one molecule per bipyramid. As argued in the main text of the paper, we however believe that crystal violet (CV) adsorption occurs only at the tips (referred here as hot-spots, HS) of the bipyramids (with 2 HS per bipyramid), and not elsewhere on the bipyramids or on the sphere. In this case a concentration of 0.5 nM of CV in solution would result in one CV/HS.

From these estimates, the number of molecules per bipyramid can be estimated by simple scaling depending on final analyte concentration and dilution of the starting colloid solution. For the samples discussed in the text, we have:

- Sample A was prepared in two steps. A solution of [200 μL of BiP + 200 μL of 20 nM CV] was first prepared. Then 400 μL water was added to 100 μL of this solution to form sample A. The resulting concentrations are therefore 2 nM for CV and 0.024 nM for the BiPs ($\times$10 dilution of the starting solution). For random adsorption onto spheres and BiP, this corresponds to $\approx$ 30 CV/BiP, which would correspond to the single molecule regime, owing to the EF distribution/hot-spot area effect. However, assuming selective adsorption at the BiP hot-spots (2 HS per BiP), it would then correspond to $\approx$ 42 CV/HS, which would correspond to the many-molecule regime. The latter was observed experimentally for CV indicating selective adsorption of CV at the BiP hot-spots.

- Sample B and C were therefore prepared to experimentally assess the SM-SERS regime using the bi-analyte SERS method. In order to reduce significantly the number of CV per BiP without having to resort to extremely low CV concentrations (which are inherently prone to dilution errors), the final BiP concentration was increased by reducing the dilution factor. Also, the Nile Blue concentrations were chosen as 10 times larger than the CV concentrations to compensate for the lower adsorption at hot-spots and result in $\approx 1:1$ ratio of SM-SERS events. Sample B was prepared in two steps. A solution of [200 μL of BiP + 200 μL of 20nM NB] was first prepared. Then 315 μL water and 15 μL of 20 nM CV were added to 300 μL of this solution to form sample B. The resulting concentrations are therefore 0.5 nM (CV), 5 nM (NB) and 0.06 nM for the BiPs ($\times 4$ dilution of the starting solution). Assuming selective adsorption at the BiP hot-spots, it corresponds to ≈ 4 CV/HS, which would correspond to the intermediate regime of SMSERS.

- Similarly, Sample C was prepared in two steps, again in such a way as to minimize dye dilution errors. A solution of [1160 μL of water + 400 μL of 20 nM NB + 40 μL of 20 nM CV] was first prepared. Then 250 μL of the BiP solution was added to 250 μL of this solution to form sample C. The resulting concentrations are therefore 0.25ṅM (CV), 2.5 nM (NB) and 0.12 nM for the BiPs ($\times 2$ dilution of the starting solution). Assuming selective adsorption at the BiP hot-spots, this now corresponds to ≈ 1 CV/HS.

Finally, we note that although these estimates are useful to fix ideas, there remain subject to uncertainties. For example, they assume that CV adsorbs with 100% efficiency, which may not be the case in the presence of the CTAB layer. Moreover, at such low concentrations, wall adsorption may reduce the effective CV concentration in solution. These estimates should therefore be viewed as upper estimates of the real concentrations.

S.IV. SERS EXPERIMENTS AND ENHANCEMENT FACTORS

Experimental details

The SERS spectra were acquired with a Horiba Jobin-Yvon Labram Raman spectrometer equipped with a Synapse CCD allowing fast acquisition (read-out time of 70 ms between spectra). Excitation was provided by a 633 nm HeNe laser with a maximum power of 10 mW at the sample, which can be reduced using neutral density filters. Raman spectra were measured in solution in the backscattering configuration using a x100 (NA 1.0) water immersion objective.

Average enhancement factor

As discussed in Ref. 6, a convenient definition for the average SERS EF, especially in solution, is the so-called Analytical EF (AEF) defined as:

$$\mathrm{AEF} = \frac{I_{\mathrm{SERS}}/c_{\mathrm{SERS}}}{I_{\mathrm{RS}}/c_{\mathrm{RS}}}, \tag{S1}$$

where I_{SERS} and I_{RS} are the SERS and normal Raman intensities, respectively, measured for the same analyte under identical experimental conditions, except for a possible difference in analyte concentration (denoted c_{SERS} and c_{RS}, respectively). The AEF is relatively easy to measure experimentally (provided normal Raman spectra can be obtained), but may not be a reliable measure of the intrinsic performance of the SERS substrate [6]. It is for example dependent on the analyte adsorption efficiency, the presence of multilayer coverage, or photobleaching, and therefore only provides an upper limit of the average SERS EF.

Although it is usually not possible to measure the Raman spectrum of resonant dyes because of the overwhelming fluorescence signal, this is not the case for CV at 633 nm thanks to its extremely low fluorescence quantum yield [7]. Its Raman cross-section can therefore be determined using standard methods [6]. The AEF of CV Raman peaks can therefore be determined by estimating the effective cross-section of the average SERS spectrum (against a reference). We provide the details of the procedure on a specific example below:

- We consider Sample A, with a final CV concentration of $c_{\mathrm{SERS}} = 2$ nM. We measured a time series of 1000 SERS spectra with a power of P=1 mW and integration time of $\tau = 20$ ms. In the average spectrum, the 1620 cm^{-1} SERS peak intensity is estimated from a Pseudo-Voigt profile fit to be 180 cts, or equivalently $I_{\mathrm{SERS}} = 9 \times 10^3$ cts/s/mW (see Figure 3a of the main text).

- For the same optical set-up (i.e. same objective, grating, etc), we measured the Raman spectrum of our reference 2-bromo-2-methylpropane (2B2MP) and found the intensity of the Raman mode at 516 cm^{-1} to be $I_{\mathrm{2B2MP}} = 1.5 \times 10^4$ cts/s/mW. This mode has a differential Raman cross-section of $d\sigma_{\mathrm{2B2MP}}/(d\Omega) = 5.4 \times 10^{-30}$ cm^2/sr (at 633 nm) and the 2B2MP concentration is $c_{\mathrm{2B2MP}} = 8.76$ M.

- In addition, the normal Raman cross-section of the 1620 cm^{-1} mode of CV was measured to be [6] $d\sigma_{RS}/(d\Omega) = 3.6 \times 10^{-26}$ cm^2/sr (at 633 nm). We therefore deduce the AEF for this mode from the formula:

$$\mathrm{AEF} = \frac{I_{\mathrm{SERS}}/c_{\mathrm{SERS}}}{(I_{\mathrm{2B2MP}}/c_{\mathrm{2B2MP}})\left(\frac{d\sigma_{1620}}{d\Omega}/\frac{d\sigma_{\mathrm{2B2MP}}}{d\Omega}\right)} \tag{S2}$$

  which therefore gives $\mathrm{AEF}_{1620} \approx 4 \times 10^5$ in this particular case.

Influence of Photo-bleaching

In order to assess the possible influence of photobleaching on the SERS results [8], further SERS measurements were carried out on Sample A (final CV concentration of $c_{\mathrm{SERS}} = 2\,\mathrm{nM}$) as a function of incident laser power. The average SERS intensities of the $1620\,\mathrm{cm}^{-1}$ peak of CV were obtained in each case and normalized to integration time and laser power. The results are summarized in Table **S.I**. The SERS intensity scales linearly (within experimental uncertainty) with power from 0.01 to 1 mW, which indicates that photobleaching effects are not present up to at least 1 mW of incident laser power (for our experimental conditions). A small decrease in the SERS intensity is visible for 10 mW, possibly indicating the onset of the appearance of photo-bleaching. All experiments were therefore performed at a laser power of 1 mW.

Supplementary Table S.I: SERS intensity of the $1620\,\mathrm{cm}^{-1}$ peak of CV for sample A as a function of laser power.

Power [mW]	Int. time [ms]	I_{SERS} [cts/s/mW]
0.01	100	9300
0.1	100	8300
1	20	9000
10	20	5500

Time-dependence of SERS intensities

Thanks to the low colloid concentration in sample A (0.024 nM), it is also interesting to note that we can observe the diffusion of individual bipyramids through our scattering volume over several consecutive spectra as shown in the time-dependence of Fig. **S4**(A) and in the example of Fig. **S4**(B). Some of these events last as long as 500 ms. The auto-correlation function of the time-dependent intensity in Fig. **S4**(A) shows an initial exponential decay with a time constant of 100 ms, which is therefore the order of the bipyramid diffusion time through the scattering volume (which has a Gaussian intensity profile with a waist diameter of $2w_0 = 1.38\,\mu\mathrm{m}$, see below). This interpretation is further confirmed from Dynamic Light Scattering (DLS) measurements of the diffusion coefficient giving $D \approx 13\,\mu\mathrm{m}^2/\mathrm{s}$, which corresponds for example to a rms displacement of $1.1\,\mu\mathrm{m}$ in 100 ms, or $2.5\,\mu\mathrm{m}$, in 500 ms. This observation further confirms the fact that the SERS signals originate from individual bipyramids (as opposed to aggregates).

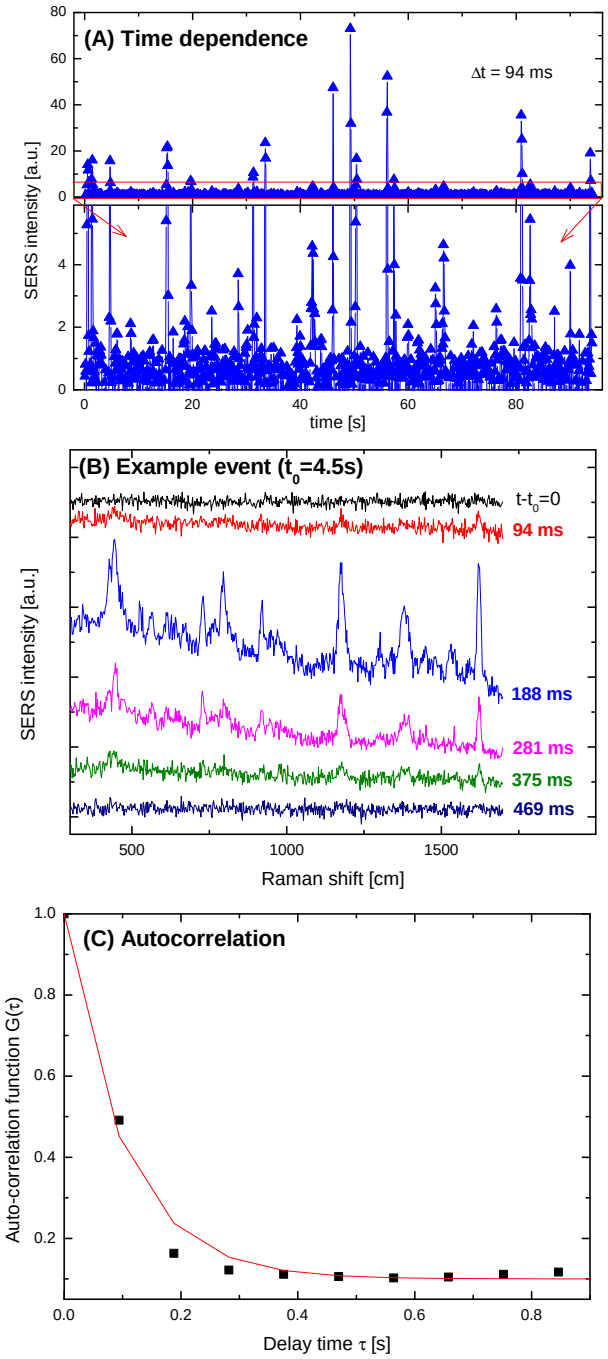

Supplementary Figure S4: (A) Time evolution SERS intensity for sample A obtained for 1000 individual spectra (integration time $\tau = 20\,\mathrm{ms}$, taken at $\Delta t = 94\,\mathrm{ms}$ interval). The lower part provides a zoom on the lower intensity events. Thanks to low NP concentration (0.024 nM) and the short time interval, most events can be seen across several consecutive spectra, reflecting the diffusion of an individual bipyramid through the scattering volume. (B) shows the spectra (vertically translated for clarity) for such an event. (C) Autocorrelation function for the SERS intensities shown in (A) along with a fit with an exponential decay time of 100 ms. Note that the time resolution for the autocorrelation function is poor because the interval between consecutive spectra is of the order of the diffusion time.

Scattering volume characterization

In order to estimate single-molecule SERS EF, it is first necessary to characterize the scattering volume, which we did here following the method described in detail in Ref. [6]. Briefly, we first measured the Raman intensity on a silicon substrate immersed in water as a function of the confocal pinhole size. Knowing the magnification factor between the sample and the image on the pinhole, we can infer the beam waist of the exciting beam (assumed to be Gaussian) to be $w_0 = 690\,\mathrm{nm}$. Then, the confocal depth is estimated by scanning the focal plane across the Si substrate. Following the definitions of Ref. [6], we obtain an effective height of $H_{\mathrm{eff}} = 12\,\mu\mathrm{m}$ and therefore an effective scattering volume of $V_{\mathrm{eff}} = 8.2\,\mu\mathrm{m}^3$.

Single molecule SERS EF

Using this, we can again use our reference standard, 2-bromo-2-methylpropane (2B2MP), to relate the measured Raman intensity (in cts/s/mW) to an effective differential cross-section (which is the cross-section for a hypothetical single emitter in the center of the scattering volume producing the same Raman intensity). For a 2B2MP solution (with a concentration $c = 8.76\,\mathrm{M}$), the intensity of the Raman mode at $516\,\mathrm{cm}^{-1}$ was measured to be $I_{\mathrm{2B2MP}} = 1.5 \times 10^4\,\mathrm{cts/s/mW}$, which must therefore correspond to an effective cross-section of $cV_{\mathrm{eff}} \times d\sigma_{\mathrm{2B2MP}}/(d\Omega)$. We conclude that for the experimental conditions used in this work, we have:

$$1\,\mathrm{cts/s/mW} \quad \Leftrightarrow \quad 1.7 \times 10^{-23}\,\mathrm{cm}^2/\mathrm{sr} \qquad \text{(S3)}$$

For a given Raman spectrum, this relation can then be used to convert the Raman intensity of, for example, the $1620\,\mathrm{cm}^{-1}$ mode of CV into a differential cross-section. Normalizing with the normal Raman cross-section of the same mode, $d\sigma_{RS}/(d\Omega) = 3.6\times10^{-26}\,\mathrm{cm}^2/\mathrm{sr}$ (at 633 nm), we then obtain an equivalent SM-SERS enhancement factor. It is important to note that this equivalent SM-SERS EF is only a real SM-SERS EF if it is proven that the Raman spectrum indeed originates from a single molecule.

As an example, the Raman intensity of the $1620\,\mathrm{cm}^{-1}$ mode of CV in the SM-SERS of Fig. 3e in the main text is $I_{1620} = 640\,\mathrm{cts}$ with 0.1 s integration time at 1 mW, or equivalently $I_{1620} = 6400\,\mathrm{cts/s/mW}$. This therefore corresponds to an effective differential cross-section of $1.1 \times 10^{-19}\,\mathrm{cm}^2/\mathrm{sr}$ and a SM-SERS EF of 3×10^6.

Statistical analysis of bianalyte SERS experiments

In order to analyze the bianalyte SERS experiments, good quality average spectra of CV only and NB only were obtained at higher concentrations (in samples such as sample A), to be used as reference spectra, denoted $I_{\mathrm{CV}}(\bar{\nu})$ and $I_{\mathrm{NB}}(\bar{\nu})$. Each individual spectra in the bianalyte experiment, $I_n(\bar{\nu})$ is then fitted to a linear combination of these references with a linear background, i.e.:

$$I_n(\bar{\nu}) = \alpha_n I_{\mathrm{CV}}(\bar{\nu}) + \beta_n I_{\mathrm{NB}}(\bar{\nu}) + \gamma_n \bar{\nu} + \delta_n \qquad \text{(S4)}$$

The fit is carried out as a linear least square fit and can be carried out analytically (using matrix algebra) and therefore very rapidly for a large number of spectra. Moreover, the resulting fitting parameters are guaranteed to be those of the absolute minimum with no local minima or convergence issues as would arise in a non-linear least square fit. The values of α_n are then converted into cts/s/mW (using the reference spectrum $I_{\mathrm{CV}}(\bar{\nu})$) and then into an equivalent SM-SERS EF as described in the previous section. This would be the SM-SERS EF experienced by a single molecule producing the same intensity as observed (and is therefore the true SM-SERS EF for single molecule events).

In practice, the fit is carried out in a limited spectral range containing strong and distinguishable Raman peaks of CV and NB. The limited spectral range is necessary to ensure that the background can be well approximated as linear and to avoid variations in relative peak SERS intensities associated with the underlying LSP resonance [9]. For the analysis presented here, the spectral range was chosen as $1550\,\mathrm{cm}^{-1} \leq \bar{\nu} \leq 1680\,\mathrm{cm}^{-1}$. The advantage of this linear least-square fit approach is that it does not rely on assumptions on the line shape of the Raman peaks and can easily handle multiple overlapping peaks. The results are very robust and are only affected by the unavoidable noise in the lower-intensity spectra, which result in non-zero (and possibly negative) small values in the parameters α_n and β_n. The minimum detectable signal-to-noise ratio is then easily identifiable in a scatter plot of α_n vs β_n as the one shown in Fig. 3b. The events below noise level are simply those whose magnitude is comparable to the maximum negative values of α_n and β_n (the green points in Fig. 3b).

[1] Liu, M. Z. & Guyot-Sionnest, P. J. Mechanism of silver(i)-assisted growth of gold nanorods and bipyramids. *J. Phys. Chem. B* **109**, 22192–22200 (2005).

[2] Etchegoin, P. G., Le Ru, E. C., & Meyer, M. An analytic model for the optical properties of gold. *J. Chem. Phys.* **125**, 164705 (2006).

[3] Pecora, R. Dynamic light scattering measurement of nanometer particles in liquids. *Journal of Nanoparticle Research* **2**, 123–131 (2000).

[4] Power, A. C., Betts, A. J., & Cassidy, J. F. Non aggregated colloidal silver nanoparticles for surface enhanced resonance Raman spectroscopy. *Analyst* **136**, 2794–2801

(2011).

[5] Bohren, C. F. & Huffman, D. R. *Absorption and scattering of light by small particles.* John Wiley & Sons Inc., New York, (1983).

[6] Le Ru, E. C., Blackie, E., Meyer, M., & Etchegoin, P. G. Surface enhanced Raman scattering enhancement factors: a comprehensive study. *J. Phys. Chem. C* **111**, 13794–13803 (2007).

[7] Galloway, C. M., Etchegoin, P. G., & Le Ru, E. C. Ultrafast nonradiative decay rates on metallic surfaces by comparing surface-enhanced Raman and fluorescence signals of single molecules. *Phys. Rev. Lett.* **103**, 063003 (2009).

[8] Etchegoin, P. G., Lacharmoise, P. D., & Le Ru, E. C. Influence of photostability on single-molecule surface enhanced Raman scattering enhancement factors. *Anal. Chem.* **81**, 682–688 (2009).

[9] Buchanan, S., Le Ru, E. C., & Etchegoin, P. G. Plasmon-dispersion corrections and constraints for surface selection rules of single molecule SERS spectra. *Phys. Chem. Chem. Phys.* **11**, 7406–7411 (2009).